(a) **(b)**

FIG. 3. (a) Magnetic field configuration before any discharge occurs. (b) Postulated magnetic field and current configurations after i_z currents have gathered both plasma and h_z field lines into discrete tubes or filaments.

Thus, from (1) and (2)

$$\phi_z/i_z = \text{const}''$$

and from (1) and (3)

$$\phi_z/i_z R = \text{const}'''.$$

Therefore for a given ϕ_z and i_z there can be one and only one equilibrium value of R. If the field h_z diverges so that the radius R "tries to swell up" the tube of flux, it is to be expected that the current will break up into n tubes where $\phi_z = n\phi_z'$, and $i_z = ni_z'$, each tube having a radius R' equal to R.

While this experiment and its analysis are both preliminary and very crude, they nevertheless indicate the tremendous potential value of such experiments in the laboratory. The experiment demonstrates the basic requirements for streamer formation and suggests an appropriate magnetic field configuration for a plasma guide. The experiment therefore not only educes evidence which supports the Alfvén[2] theory of sunspots, but also strongly suggests that a magnetohydrodynamic whirl ring has the more general current and magnetic field configuration shown in Fig. 4(b) rather than that
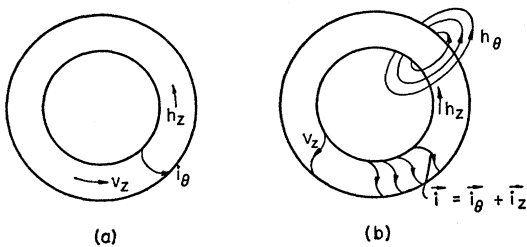

(a) **(b)**

FIG. 4. Current and field configurations for magnetohydrodynamic whirl rings, (a) as postulated by Alfvén and Walén, (b) as suggested by laboratory experiments.

proposed by Alfvén and Walén [shown in Fig. 4(a)]. The current and field configuration of Fig. 4(b) upon intersection with the sun's surface will then be expected to produce not only two sunspots with their magnetic fields but also a current which flows between the sunspots along these field lines in the sun's atmosphere. The current and magnetic-field conditions on the photosphere and in the chromosphere in the region of the sunspots will then be geometrically similar to those in the laboratory experiment where streamers are produced.

The author is indebted to Orrin Twite who executed the experimental setup and to Harold Furth with whom he had discussions concerning the mechanism of the streamer formation.

[1] W. H. Bostick, Phys. Rev. 104, 292 (1956); also Bull. Am. Phys. Soc. Ser. II, 1, 166 (1956).
[2] H. Alfvén, Cosmical Electrodynamics (Oxford University Press, New York, 1950), p. 88.

Antineutrons Produced from Antiprotons in Charge-Exchange Collisions*

BRUCE CORK, GLEN R. LAMBERTSON, ORESTE PICCIONI,† AND WILLIAM A. WENZEL

Radiation Laboratory, University of California,
Berkeley, California

THE principle of invariance under charge conjugation gained strong support when it was found that the Bevatron produces antiprotons.[1-3] Another prediction of the same theory which could be tested experimentally was the existence of the antineutron. Additional interest arises from the fact that charge conjugation has somewhat less obvious consequences when applied to neutral particles than it has when applied to particles with electric charge.

The purpose of this experiment was to detect the annihilation of antineutrons produced by charge exchange from antiprotons. Because the yield of antineutrons was expected to be low, a relatively large flux of antiprotons was required. Protons of 6.2-Bev energy bombarded an internal beryllium target of the Bevatron (Fig. 1). With a system of two deflecting magnets and five magnetic lenses a beam of 1.4-Bev/c negative particles was obtained. Six scintillation counters connected in coincidence distinguished antiprotons from negative mesons by time of flight. In Figs. 1 and 2, F is the last counter of this system, which counted 300 to 600 antiprotons per hour. Antiprotons interacting in the thick converter, X (Fig. 2), sometimes produce antineutrons which pass through the scintillators S_1 and S_2 without detection and finally interact in the lead glass Čerenkov Counter C, producing there a pulse of light so large as to indicate the annihilation of a nucleon and an antinucleon.
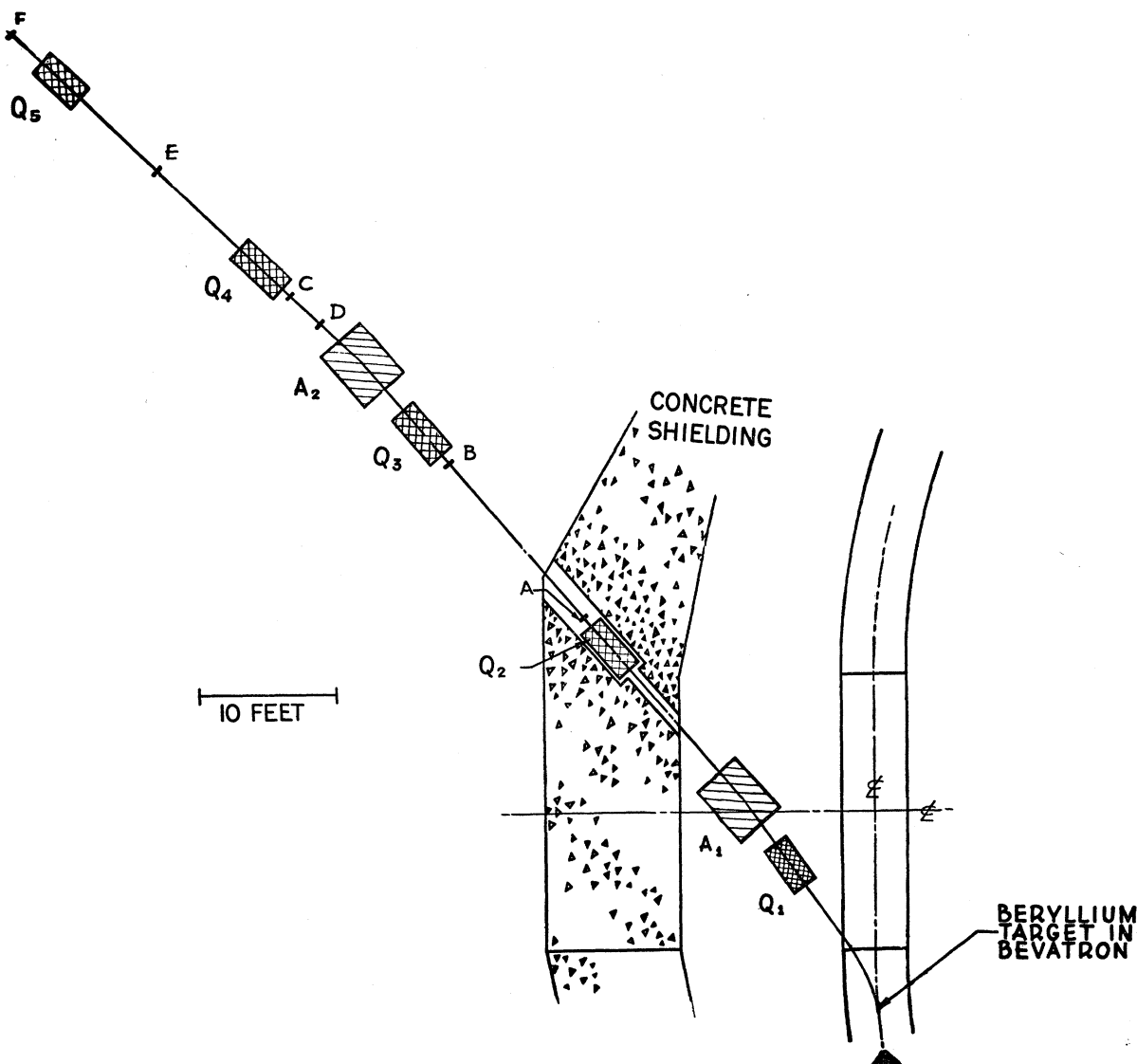
FIG. 1. Antiproton-selecting system. Q_1 through Q_5 are focusing quadrupoles. A_1 and A_2 are analyzing magnets. A through F are 4-by-4-by-$\frac{1}{4}$-inch scintillators.

The Čerenkov Counter C is a piece of lead glass, 13 by 13 by 14 in., density=4.8, index of refraction =1.8, viewed by 16 RCA 6655 photomultipliers. This instrument is similar to the one used in a previous experiment on antiprotons.[2] A 1-in. lead plate is placed between S_1 and S_2 to convert high-energy gamma rays which could otherwise be confused with the antineutrons. Ordinary neutrons and neutral mesons (heavier than pions) can be detected by the Čerenkov counter but their average light pulse is much smaller than that from the annihilation of an antineutron. However, a relatively small background of these neutral secondaries would distort the apparent spectrum of antineutrons.

To discriminate against these neutral secondaries, the charge-exchange converter, X, was made of a scintillating toluene-terphenyl solution, viewed by four photomultipliers connected in parallel. In this way neutral particles producing pulses in the Čerenkov counter ("neutral events") could be separated according to whether they originated in an annihilation, indicated by a large pulse in X, or in the less violent process expected to accompany the charge-exchange production of an antineutron. A quantitative criterion for this separation is derived from a comparison between the pulse-height spectra in X, shown in Fig. 3. The dashed curve, obtained in a separate experiment, is the spectrum produced by antiprotons passing through but not interacting in X. The sharp peak in the spectrum provides the calibration of X; the ionization loss for
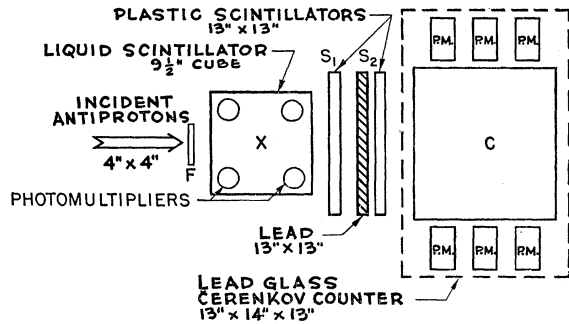
FIG. 2. Antineutron-detecting system. X is the charge-exchange scintillator; S_1 and S_2 are scintillation counters; C is a lead-glass Čerenkov counter (later a large scintillator).

FIG. 4. Pulse-height spectrum in lead glass counter for neutral events. The solid histogram is for 54 antineutron events (energy loss in charge-exchange scintillator less than 100 Mev). Dashed histogram is for 20 other neutral events. Smooth solid curve is for antiprotons and is normalized to the solid histogram.

transmitted antiprotons is readily computed to be 50 Mev. The smooth solid curve of Fig. 3, obtained with the geometry of Fig. 2, represents all antiproton interactions in X from which no pulse was observed in S_1 and S_2, whether or not a pulse in C occurred. For those events in which a neutral particle produced a pulse in C, the histogram of Fig. 3 gives the pulse-height distribution.

The difference between the solid curve and the histogram is remarkable in that it shows that the rare interactions that produce neutral particles detected by the Čerenkov counter release much less energy in X than the other unselected interactions. In fact, the peak of the histogram is at a smaller pulse height than that which corresponds to the ionization loss of a non-interacting antiproton (50 Mev). This is what we should expect if the neutral particles were antineutrons, for in this case no nucleonic annihilation could take place in X. Conversely, production of other energetic neutrals should exhibit the characteristic large pulse of an annihilation event in X. The histogram suggests, therefore, that the apparatus detects a small background of events of this latter type. The pulse height of 100 Mev in Fig. 3 has been selected to separate this background from antineutron events. Figure 4 shows the separate pulse-height distributions in the Čerenkov counter for

the events which produced in X a pulse less than 100 Mev (solid histogram), and for the events which produced a pulse larger than 100 Mev (dashed histogram). The great difference between the two histograms with respect to both average pulse height and shape confirms the interpretation by which the neutral events are divided into antineutrons and background.

The energy scale in Fig. 4 is obtained by relating the pulse height produced by π mesons going through the glass to the computed ionization energy loss of 240 Mev. This calibration was repeated every day.

The standard for annihilation pulses is provided by the smooth curve of Fig. 4, which is the pulse-height distribution for antiprotons entering the lead glass when S_1, S_2, and the lead plate are removed. Comparison of the solid histogram with this antiproton curve justifies our interpretation that the solid histogram is produced by antineutrons.

For comparison with the annihilation spectra of Fig. 4, Fig. 5 shows the spectra obtained with 750-Mev positive protons (solid curve) and with 600-Mev negative pions incident on the glass Counter C. These spectra indicate that large pulses are rarely produced by particles of such energies. From this it is apparent that even high-energy neutrons could not produce a spectrum like the solid histogram of Fig. 4.
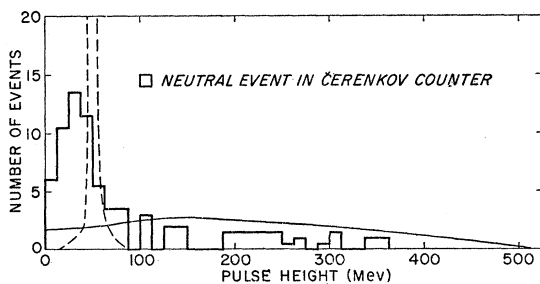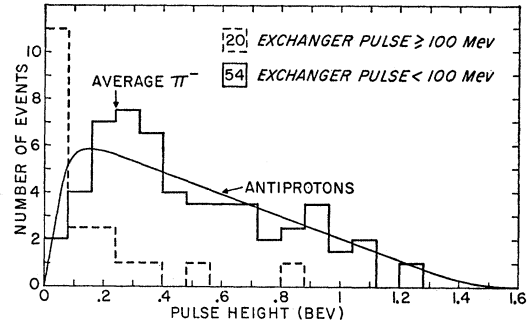

FIG. 3. Pulse-height spectrum in charge-exchange scintillator for 74 neutral events in lead glass. Histogram is for all neutral events. The smooth solid curve is for calibrating antiprotons for which no pulse occurred in S_1 or S_2. Smooth dashed curve is for noninteracting antiprotons. Smooth curves are each normalized to histogram.
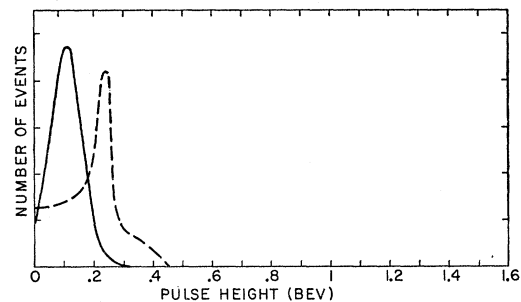

FIG. 5. Pulse-height spectrum in lead glass counter for π mesons (dashed curve) and for positive protons (solid curve). The curves are normalized.
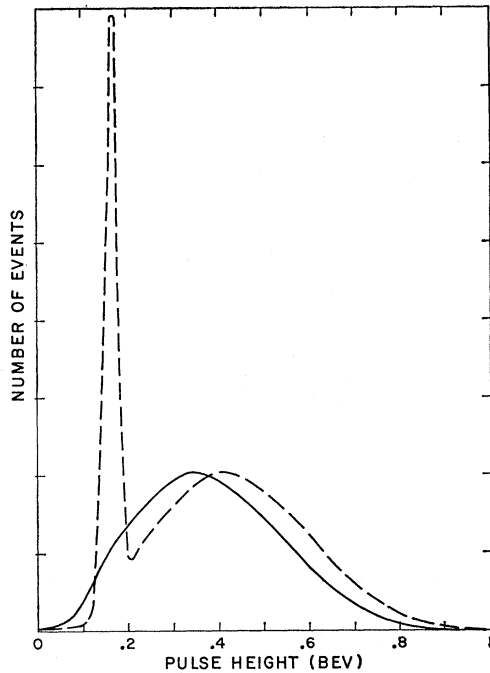
FIG. 6. Pulse-height spectrum of antiprotons in large scintillation counter. The dashed curve is for all incident antiprotons. The solid curve has had noninteracting antiprotons removed and includes a correction to permit comparison with antineutrons.
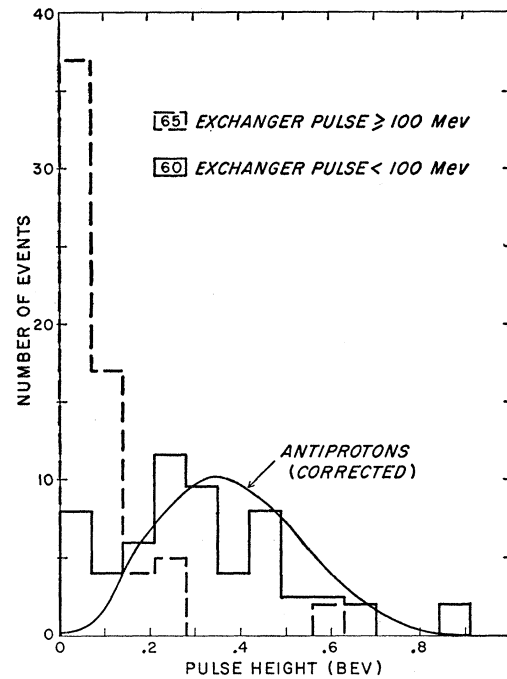

FIG. 7. Pulse-height spectrum in large scintillation counter for neutral events. Solid histogram is for 60 antineutrons (energy loss in charge-exchange scintillator less than 100 Mev). Dashed histogram is for 65 other neutral events. The smooth solid curve is the corrected antiproton curve from Fig. 6.

To determine the number of γ rays incident on S_1, the lead between S_1 and S_2 was removed. The number of neutral events per incident antiproton increased by a factor of 7. From the known probability that a single high-energy γ ray would be transmitted through 1 in. of lead without converting (3% for a γ-ray energy of 300 Mev), this observed increase shows that our neutral events contain at most 20% of γ-ray background before selection on the basis of pulse height in X.

The lead glass Counter C is very sensitive to γ rays and insensitive to ionization losses by slow particles. The desirability of comparing the spectra of anti-neutrons and antiprotons obtained with an entirely different type of detector led us to repeat the experiment with Counter C replaced by a liquid scintillator. This scintillator, 28 in. thick and 5 ft³ in volume, was large enough to detect a substantial part of the energy of an annihilation event. For this experiment the thickness of the lead converter between S_1 and S_2 was increased to 1.5 in. As before, the antineutron detector was calibrated with antiprotons. The pulse-height distribution of antiprotons in the large scintillator is given by Fig. 6. The noninteracting antiprotons produce the sharp peak.

The solid smooth curve in Fig. 7 is the solid curve of Fig. 6, obtained by correcting the pulse height by 70 Mev toward lower energy because antiprotons ionize before interacting in the scintillator. Sixty neutral events were obtained (Fig. 7) after selection with the

same criterion as before on the pulse height in X. Again the selected neutral spectrum and the antiproton spectrum are in agreement, although not so strikingly as with the lead glass. The sixty selected events apparently include some contamination. This interpretation is confirmed by the shape of the spectrum in X for all neutral events (Fig. 8). There are now many more neutral secondaries from inelastic collisions of antiprotons than there were in the experiment with the lead glass, and the separation between antineutrons and background is therefore not so good. The larger number of neutral secondaries is probably to be attributed to the greater sensitivity of the scintillator to neutrons.

The lead glass and the scintillator are of nearly equal efficiency in detecting the antineutrons. The observed
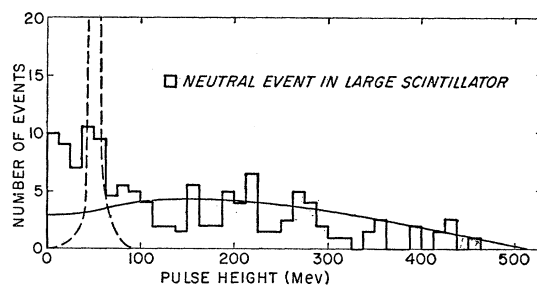

FIG. 8. Pulse-height spectrum in charge-exchange scintillator for 125 neutral events in large scintillator. The smooth curves are the same as in Fig. 3, each normalized to histogram.

yield from about 20 g/cm² of toluene is 0.0030±0.0005 antineutrons per antiproton with the lead glass, and 0.0028±0.0005 with the liquid scintillator. With the assumption that the interaction cross section for antineutrons is the same as for antiprotons, the inefficiency of the detector due to attenuation in S_1, S_2, and the lead converter, and to transmission of the detector can be calculated, and is found to be about 50%. From the observed antineutron yield the mean free path for charge exchange of the type detected is about 2300 g/cm² of toluene (C_7H_8); or, in other words, the exchange cross section is about 2% of the annihilation cross section for this material. This corresponds to a cross section of approximately 8 millibarns in carbon for this process.

The generous support of many groups, including the Bevatron operating group under Dr. Edward J. Lofgren, is greatly appreciated.

We thank Professor David Frisch of Massachusetts Institute of Technology for the loan of the lead glass used in the Čerenkov counter.

† On leave of absence from Brookhaven National Laboratory, Upton, New York.
[1] Chamberlain, Segrè, Wiegand, and Ypsilantis, Phys. Rev. **100**, 947 (1955).
[2] Brabant, Cork, Horwitz, Moyer, Murray, Wallace, and Wenzel, Phys. Rev. **101**, 498 (1956).
[3] Chamberlain, Chupp, Ekspong, Goldhaber, Goldhaber, Lofgren, Segrè, Wiegand, Amaldi, Baroni, Castagnoli, Franzinetti, and Manfredini, Phys. Rev. **102**, 921 (1956).

Magnetic Moment of the Proton in Bohr Magnetons*

PETER FRANKEN† AND SIDNEY LIEBES, JR.

Department of Physics, Stanford University, Stanford, California
(Received September 18, 1956)

THIS note is a brief report on a recent measurement of the magnetic moment of the proton in units of the Bohr magneton. The nuclear magnetic resonance frequency, $\omega_p = 2\mu_{p(\mathrm{oil})}H/\hbar$, of protons in mineral oil and the cyclotron frequency, $\omega_e = eH/mc$, of free low-energy electrons are measured in the same magnetic field H. The ratio of these two frequencies yields the proton moment in Bohr magnetons, $\omega_p/\omega_e = \mu_{p(\mathrm{oil})}/\mu_0$, uncorrected for environmental shifts due to the mineral oil.

In the previously reported measurements of the proton moment by the electron-cyclotron method,[1,2] one of the important limitations on accuracy was imposed by shifts in the electron-cyclotron frequency arising from the presence of nonvanishing radial electrostatic fields. These fields can be produced by space charge, externally applied trapping voltages, or stray charges accumulating on the boundaries of the system in which the resonance is studied. The present experiment is specifically designed to correct for these shifts

in a fashion that does not require a quantitative knowledge of the electrostatic field distribution.

We make three assumptions which are subjected to experimental verification: (1) The electron orbit radii are small compared to distances in which the electrostatic field varies appreciably. (2) The frequency shift caused by the electrostatic field is small. (3) The electrostatic field is independent of magnetic field in a chosen range of magnetic field variation.

When assumptions (1) and (2) obtain, it follows that the fractional shift of the observed cyclotron frequency ω_e', relative to the unshifted frequency ω_e, is, in Gaussian units,

$$\frac{\omega_e' - \omega_e}{\omega_e} = \frac{c\bar{E}_r}{v_\perp H} = \left[4\pi\rho - \left(\frac{\partial E_z}{\partial z}\right)_0\right]\frac{mc^2}{2eH^2}, \qquad (1)$$

wherein $\bar{E}_r = (1/2\pi)\int_0^{2\pi} E_r d\theta$ represents the average radial electric field at the orbit, $v_\perp$ the magnitude of the component of the electron velocity perpendicular to the direction of the magnetic field, and ρ the space charge density. The electric field derivative is evaluated at the orbit center and the direction of H is chosen parallel to the z-axis. We take $e > 0$.

The experimentally observed quantity ω_e'/ω_p can be related to $\mu_0/\mu_{p(\mathrm{oil})}$ by the expression

$$\frac{\omega_e'}{\omega_p} = \frac{\mu_0}{\mu_{p(\mathrm{oil})}}\left\{1 + \left[4\pi\rho - \left(\frac{\partial E_z}{\partial z}\right)_0\right]\frac{mc^2}{2eH^2}\right\}. \qquad (2)$$

The absence of any orbit or velocity parameters in (2) suggests the measurement of ω_e'/ω_p as a function of magnetic field. If assumption (3) is satisfied in the range of variation of H, one should observe a linear dependence of ω_e'/ω_p with respect to $1/H^2$. A linear extrapolation to $(1/H^2) = 0$ determines $\mu_0/\mu_{p(\mathrm{oil})}$.
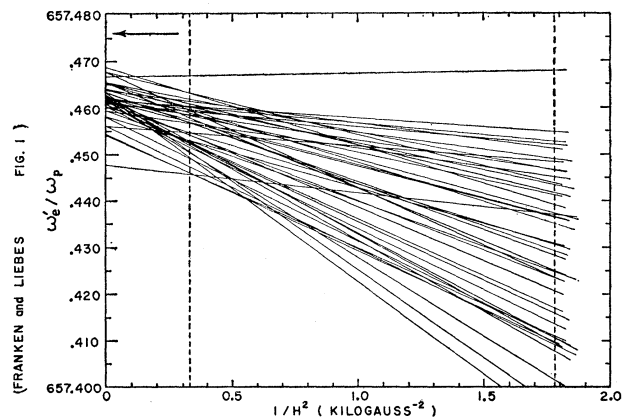

FIG. 1. ω_e'/ω_p, for a spherical sample of mineral oil, is plotted *versus* $1/H^2$ for each run. The straight lines represent least-squares fits to the data of each run. The vertical dashed lines indicate the interval of magnetic field variation in which the data were taken. The heavy horizontal arrow at 657.476 indicates the terminal value of ω_e'/ω_p for zero-energy electrons that should have been obtained in order to yield the theoretical value for the magnetic moment of the free electron.